NASA Technical Memorandum 106426
IEPC–93–108

Performance of the NASA 30 cm Ion Thruster

Michael J. Patterson and Thomas W. Haag
Lewis Research Center
Cleveland, Ohio

and

Scot A. Hovan
University of Dayton
Dayton, Ohio

Prepared for the
23rd International Electric Propulsion Conference
cosponsored by the AIAA, AIDAA, DGLR, and JSASS
Seattle, Washington, September 13–16, 1993

NASA

IEPC-93-108

Performance of the NASA 30 cm Ion Thruster

Michael J. Patterson* and Thomas W. Haag*
National Aeronautics and Space Administration
Lewis Research Center
Cleveland, Ohio

Scot A. Hovan
Department of Mechanical Engineering
University of Dayton
Dayton, Ohio

A 30 cm diameter xenon ion thruster is under development at NASA to provide an ion propulsion option for missions of national interest, and is being proposed for use on the USAF/TRW Space Surveillance, Tracking and Autonomous Repositioning (SSTAR) platform to validate ion propulsion. The thruster incorporates innovations in design, materials, and fabrication techniques compared to those employed in conventional ion thrusters. Specific development efforts include thruster design optimizations, component life testing and validation, vibration testing, and performance characterizations. Under this test program, the ion thruster will be brought to engineering model development status. This paper discusses the performance and power throttling test data for the NASA 30 cm diameter xenon ion thruster over an input power envelope of 0.7 to 4.9 kW, and corresponding thruster lifetime expectations.

Nomenclature

A_{oaa} = accelerator grid open area, m^2
F = thrust, N
F_t = thrust-loss correction factor due to off-axis vectoring
f_{oaa} = physical open-area-fraction of accelerator grid
g = acceleration due to gravity, m/s^2
I_{sp} = specific impulse, s
I^+ = singly-charged ion beam current, A
I^{++} = doubly-charged ion beam current, A
J_a = accelerator grid impingement current, A
J_b = ion beam current, A
J_d = discharge (anode) current, A
J_{nk} = neutralizer keeper current, A
J_s = screen current, A
j^+ = singly-charged ion current density, A/m^2
j^{++} = doubly-charged ion current density, A/m^2
M = propellant atomic mass unit
M_i = propellant ingested flow, eq. A
M_o = total propellant flow rate, eq. A
m = ion mass, kg
m_c = discharge cathode propellant flow rate, sccm
P_{inpt} = thruster input power, W
q = ion charge, C
R = net-to-total voltage ratio
R_{scrn} = internal erosion rate of screen grid
T_{pc} = corrected facility pressure, Pa
V_a = accelerator grid voltage, V
V_b = beam voltage, V
V_d = discharge (anode) voltage, V
V_g = floating potential of neutralizer-common with respect to facility ground, V
V_{nk} = neutralizer keeper voltage, V
V_s = screen grid voltage, V
$Y(E)$ = sputter yield due to ion bombardment at energy E
α = thrust-loss correction factor for doubly-charged ions
γ = total thrust-loss correction factor
η_t = total thruster efficiency
η_u = total propellant utilization efficiency
ϕ_s = screen grid transparency to ions

*Aerospace Engineer, Member AIAA

PERFORMANCE OF THE NASA 30 CM ION THRUSTER

Introduction

There are potential near-term missions, including orbit-raising, station-keeping, and satellite repositioning that may benefit from the use of ion propulsion. These benefits may be derived in a number of ways including reduced launch mass, and/or increased on-orbit lifetime. Several flight experiments and demonstrations of ion propulsion are being conducted by the Europeans and Japanese during this decade.[1-3] In the United States, NASA has a program to develop ion thruster system technologies to satisfy auxiliary and primary propulsion requirements on missions of national interest.

One potential near-term mission opportunity is NASA participation in the joint U.S. Air Force/TRW Space Surveillance, Tracking and Autonomous Repositioning (SSTAR) program. Under this program NASA would supply an Ion Propulsion Subsystem (IPS) that would be flown as a secondary payload using SSTAR as the carrier. The SSTAR spacecraft is designed to test key technologies associated with the development of electric orbit transfer vehicles (EOTV) and includes 10 kW of solar array power and an ammonia arcjet propulsion system. The IPS would consist of the NASA 30 cm ion thruster, a power processor, a xenon feed system, and a diagnostics instrumentation package. The preliminary mission plan calls for operating the IPS at a nominal 2.5 kW power level to demonstrate repositioning and orbit transfer, and to evaluate IPS performance and interactions with other spacecraft engineering subsystems.

To date, a series of test programs has been conducted at NASA with laboratory version 30 cm ion thrusters and components to establish a database for development of an engineering model thruster. These include identifying wear mechanisms and design modifications at 5 and 10 kW power levels[4,5]; establishing baseline performance on xenon and krypton propellants[6,7]; evaluating alternative discharge chamber, ion optics, and neutralizer designs[8-11]; determining performance and lifetime limits at low ($\leq$ 2000 s) specific impulse[12]; conducting wear testing of hollow cathodes[13,14]; and evaluating the implications of derating the 30 cm ion thruster for use on power-limited spacecraft.[15,16]

An activity is now underway to develop an engineering model 30 cm xenon ion thruster, and it is in support of the ground-based testing phase for the SSTAR program. The goals of this effort are to develop a thruster with the following attributes:

compatibility with the mission requirements of both auxiliary and primary propulsion functions;

capability of operating over an input power envelope of 0.5-to-5.0 kW with 10,000 h lifetime;

reduced size, mass, parts count, and fabrication costs from state-of-the-art, and;

simplified thruster operation and interfaces.

Additionally NASA is pursuing the transfer of this technology to U.S. industry via loans of thruster system hardware and drawing packages.

The activities to develop an engineering model thruster include thruster design optimizations, development of a Computer-Aided-Design (CAD) thruster drawing package, thruster component life testing and validations, vibration testing, and thruster performance characterizations. These activities are to conclude with more detailed characterizations of the thruster interfaces including quantifying power processing requirements and conducting electromagnetic compatibility measurements with functional and engineering model thruster hardware. Thruster wear tests to demonstrate life requirements, and integration tests with breadboard power processor units will be conducted.

This paper discusses the performance of the NASA 30 cm ion thruster on xenon propellant over an input power range of 0.7 to 4.9 kW, and corresponding lifetime expectations.

Thruster Design

The thruster hardware, shown in Figures 1 and 2, is presently developed to a functional model status. It has a configuration similar to that which may be used in a flight application, and is being used to verify the physical and functional design, and to define manufacturing processes. This will be followed by an engineering model thruster, depicted in Figure 3, that will be used to validate the design and prove readiness for production.

The functional model xenon ion thruster was developed with certain operational and performance goals and objectives. These include: an input power envelope of 0.5 kW to 5.0 kW, with a lifetime of 10,000 h; performance comparable to that demonstrated previously with 30 cm laboratory model thrusters[4-6,8,10,12]; design and interfaces that are compatible with the mission and system requirements for both auxiliary and primary propulsion applications; simplified power processing requirements; and reduced thruster size, mass (to approximately 7 kg), parts

count, and fabrication costs. Some of the primary design objectives for the thruster are summarized in Table I.

The functional model thruster of Figs. 1 and 2 incorporates innovations in design, materials, and fabrication techniques compared to those employed in conventional thrusters. These include:

The thruster is designed with a conic discharge chamber, which transitions into a short cylindrical region immediately upstream of the ion optics. This partial-conic design is inherently more rigid and occupies less volume than conventional cylindrical shape thrusters which use large, flat circular rear walls, while still exhibiting good discharge characteristics and promoting a uniform plasma distribution across the exit plane. Past development efforts have shown the large rear wall of cylindrical shape thrusters to be an inefficient stress-bearing structure, and vulnerable to mechanical vibration.[17]

The use of non-ferromagnetic discharge chamber materials is a major departure from conventional ring-cusp thruster designs, and previous NASA 30 cm laboratory -version thrusters. The functional model thruster uses 0.8 mm thick alloy 1100 aluminum for the discharge chamber, magnet retention rings, and other structural components. The use of aluminum, as opposed to steel, was motivated by a concern to reduce the thruster mass to an absolute minimum. This is because thruster mass reductions can create a 'ripple' effect that can significantly reduce the mass of a multi-thruster propulsion system.[16] An added advantage of aluminum is that the complex shape of the thruster can be readily fabricated using a spin forming technique, at relatively low cost. Both die stamping and spin forming were originally considered as each technique permits seamless formation of complex shapes from a single sheet of metal. Because of its lower initial tooling cost, metal spinning is often preferred for low volume production, and was used for fabricating the thruster aluminum components described herein. While other aluminum alloys would be considerably stronger, alloy 1100 is more commonly used in spin forming because it is soft and can be shaped quickly. Higher strength metals can be spun in a similar way but need periodic annealing and may possibly require use of a steel mandrel. This added expense was judged unnecessary for a functional model thruster and so 1100 aluminum was selected. It is anticipated that the engineering model thruster will incorporate alloy 5086 aluminum, or equivalent.

The discharge hollow cathode does not employ a keeper or starting electrode and discharge-coupling to the anode is used for ignition and steady-state operation. With the screen grid electrode electrically isolated, all cathode potential surfaces in the discharge chamber, except the hollow cathode assembly itself, are eliminated in the thruster design. This approach reduces the total number of components subjected to sputtering via discharge plasma ions to an absolute minimum.

The thruster uses a distributed 'reverse-injection' propellant manifold for the discharge chamber flow. The reverse-feed approach improves the propellant efficiency obtainable especially at throttled conditions, as compared to the conventional approach of introducing the propellant at the rear of the discharge chamber.

The functional model thruster is designed to accommodate a simplified power processing approach. The thruster is normally operated using 4 commercial power supplies for steady-state operation, with 2 additional power supplies required for starting, with a total of 7 power leads to the thruster. This is a factor of 2 reduction in number of power supplies required for operation of typical xenon ion thrusters. The breadboard power processor now under development will require only a total of 3 power supplies to operate the thruster. This further reduction in power processing requirements is implemented by combining functions performed by multiple power supplies into single custom modules, with the benefit of reduced parts count and mass.[18]

The magnetic circuit employed in the thruster is of ring-cusp design.[8] It uses high-field strength, rare-earth permanent magnets in rings of alternating polarity along the perimeter of the chamber, with the field lines terminating on anode potential surfaces. Three cusps are located in the discharge, one each in the regions of the discharge cathode, the discharge sidewall (at the conic-cylinder intersection), and the ion optics-end.

The discharge chamber and neutralizer cathode assemblies are similar to those implemented in previous laboratory model ring-cusp thrusters, and used in wear tests.[4,11-15] They each consist of a hollow cathode subassembly composed of a high temperature refractory alloy tube and an electron emitting insert impregnated with a low-work

function compound. Both assemblies also use a swaged heater design derived from the mercury ion thruster, used for both activation and ignition of the cathodes. The neutralizer cathode assembly incorporates an enclosed-keeper electrode design to improve gas efficiency, with critical design parameters established to maximize ion transparency and reduce beam-coupling potentials.

The thruster ion optics system is a two-grid design developed previously for an engineering model mercury ion thruster.[17] The electrodes are fabricated from molybdenum, and have nominal thicknesses of 0.38 mm for both the screen and accelerator grids. The apertures are of cylindrical shape, with inner circle diameters of 1.91 mm and 1.14 for the screen and accelerator grids, respectively. The open-area-fraction of the screen grid is 0.67, and 0.24 for the accelerator grid. The nominal cold grid gap is set at 0.66 mm. The electrode geometries for the optics are listed in Table II.

For purposes of performance characterizations and wear testing, the functional model thruster uses a low-pressure high-voltage isolator approach. This approach results in a more complex thruster/propellant system interface than a high-pressure design, but readily permits flow variations to accommodate throttling. A modified cryogenic electrical break, designed for use with liquid nitrogen lines, accommodates the thruster high-voltage propellant isolator requirements for both low-pressure and high-pressure applications. The cryogenic break, with external dimensions of 0.64 cm diameter and 2.2 cm length, when packed with ceramic beads, can withstand at least 2.5 kilovolts operating at low-pressure conditions on xenon, and at least 3 kilovolts at high-pressure (nominally one atmosphere).[19] These devices are also implemented as low-cost, ultra-high vacuum low-voltage isolators for life testing of thruster hollow cathodes.

The selection of a high-voltage propellant isolator approach - either high-pressure, or low-pressure fed - is contingent on whether the propellant flow rate must be varied during thruster operation, how much volume is available on the thruster to accommodate feed system elements, and where the thruster/propellant system interface is drawn. The flow rates to the thruster may require active variation to accommodate power-throttling of the thruster, and/or to augment flow rates to the discharge and neutralizer cathodes during ignition. The approach that will be implemented on the engineering model thruster is dependent on results from on-going propellant isolator studies, investigations of the starting characteristics of the discharge and neutralizer cathodes, and on the SSTAR mission requirements.

Support Equipment and Procedure

Laboratory power supplies were used for thruster performance testing.[4,5] As mentioned previously, the functional model thruster uses only 4 power supplies for steady-state operation, with 2 additional power supplies for the start-up of discharge and neutralizer cathodes. A total of 7 power leads run to the thruster. The thruster does not use a discharge cathode keeper or starting electrode. Discharge ignition was routinely obtained using open circuit voltage ($\leq$ 75 volts) of the discharge supply to initiate the cathode to anode discharge. Typical starting voltages for the neutralizer were $\leq$ 20 volts.

Tests were performed using high-purity xenon propellant. The propellant feed system used an all-electropolished stainless-steel tubing construction consisting of welds and metal-gasket seals. The 3 feed lines to the thruster (main, cathode, and neutralizer) incorporated individual commercial mass flow transducers to measure the propellant flow rate. Each transducer was calibrated using a primary standard.

Thruster performance testing was conducted in the Tank 5 vacuum chamber facility at Lewis Research Center (LeRC). The chamber is 4.6 m in diameter by 19.2 m in length. The pumping characteristics of the facility include a nominal 110 kℓ/s xenon pumping speed, a no-load pressure of $\leq 6.7 \times 10^{-5}$ Pa, and an operational pressure of $\leq 1.0 \times 10^{-3}$ Pa.

The thruster was operated under manual control for all performance testing. Data were recorded from calibrated digital metering. All thruster performance data were corrected for thrust losses associated with beam divergence and doubly-charged ions. Total efficiency and specific impulse calculations included losses associated with accelerator drain and neutralizer power, and neutralizer flow rate. All propellant efficiencies included a correction to the mass flow rate for propellant ingested from the facility. A detailed discussion of the thruster performance calculations can be found in Appendix A. Estimates of critical component erosion rates, and thruster lifetimes, were made for thruster operating conditions using the method described in Appendix B.

Discharge chamber performance was obtained at fixed discharge voltage and beam current conditions. These data were taken to identify the optimum discharge operating condition for a given beam current. This optimum condition was defined to be the 'knee' of the discharge losses versus propellant efficiency curve.

Thruster Test Results

Performance data for the thruster were obtained over a 0.7-4.9 kW power envelope. Tests were conducted to: verify the performance of the aluminum, partial-conic discharge chamber design and evaluate stability; quantify overall thruster performance, and; evaluate power throttling at fixed mass flow rate conditions.

Discharge Performance

Bench-test measurements indicated a reduced internal magnetic flux density with the aluminum partial-conic discharge chamber design as compared to the conventional cylindrical-steel designs employed in previous laboratory version thrusters. Hence reduced discharge chamber, and overall thruster, performance was originally anticipated as a trade-off for reduced mass, although the magnitude of the potential performance degradation could not be quantified a priori.

Initial discharge chamber performance data indicated a high sensitivity of discharge voltage-to-cathode flow rate.[20] It was identified that factor-of-two variations in cusp field strengths at the sidewall and ion optics-end cusps had no impact on discharge stability or electrical efficiency. However, modest (30-40%) variations in the magnetic field strength in the region of the discharge cathode resulted in order-of-magnitude changes to the discharge stability, as measured by the sensitivity of the discharge voltage to variations in cathode flow rate. A change in the magnetic circuit in the region of the discharge cathode was therefore employed to improve the discharge stability.

Figures 4 and 5 show the sensitivity of the discharge voltage and beam current, and the thruster efficiency and specific impulse, to variations in cathode flow rate about a nominal 2.4 kW input power/3400 s specific impulse/1.8 A beam current operating condition for this thruster. The sensitivity of the discharge voltage and beam currents are -12.0 V/sccm, and -0.46 A/sccm, respectively. Although the discharge voltage sensitivity is approximately a factor of 2 higher than that experienced with previous NASA 30 cm laboratory version thrusters, the corresponding beam current sensitivity compares favorably to both NASA and Hughes[21] 30 cm thrusters. The data were obtained with a 1.52 mm orifice diameter discharge cathode, which is larger than that required for the cathode emission current of 12.2 A at the 2.4 kW condition. It is not known what, if any, impact there would be on sensitivity with a smaller orifice cathode. However, there were no indications that the discharge cathode was operating at too low of a temperature. At this input power, the overall thruster efficiency is 0.63-0.65 at 95 mN thrust. Typical discharge chamber performance at this condition is 200 W/A discharge losses at 0.90 total corrected discharge propellant efficiency.

The sensitivities of the discharge and thruster parameters to variations in cathode flow rate decrease with decreasing beam current, as is typical. The discharge voltage and beam current sensitivities at 1.1 A beam current at the same specific impulse/total voltage conditions of the previous 2.4 kW condition are -5.6 V/sccm, and -0.11 A/sccm, respectively, and compare favorably to other NASA and Hughes laboratory version 30 cm thrusters.

Figures 6 and 7, show the performance sensitivities at a 0.53 kW/0.8 A beam current operating condition. Note in Fig. 7 the drop-off in thruster efficiency going down in cathode flow rate below 2.0 sccm. This occurs because the correction for doubly-charged ion content is a function of the discharge propellant efficiency, and as the cathode flow rate is dropping the discharge propellant efficiency rapidly increases. Hence the estimated doubly-charge ion content of the beam increases resulting in larger thrust losses which in turn decreases the overall thruster efficiency.

Table III compiles the thruster performance sensitivities to variations in the cathode flow rate for each of four target performance conditions. Note that except for the discharge voltages, the magnitudes of all derivatives drop with decreasing beam current. The reason for the behavior of the discharge voltage derivative has to do with the selection of the operating discharge voltage at each condition (it was not constant, nor monotonic - at 1.8 A and 1.1 A beam currents, the discharge voltages were 30 and 29 volts respectively, and at 0.8 A/0.86 kW and 0.8 A/0.53 kW they were 30 and 33 volts respectively). The data of Table III are shown in Figures 8 and 9.

As a point of comparison, Figures 10 and 11 show discharge voltage and beam current derivatives as a function of beam current for the functional model thruster (from Table III), for a Hughes 30 cm laboratory version thruster (from Ref. 21), and for a NASA 30 cm laboratory version thruster. Although the discharge voltage derivatives are considerably higher for the functional model thruster than for the Hughes or NASA laboratory version thrusters, the differences in beam current derivatives are not as pronounced. Although the discharge voltage/cathode flow rate derivatives are high, the functional model thruster performance stability, as measured by the specific impulse and efficiency sensitivities to variations in cathode flow rate, compares favorably to other thrusters. Additional tests to improve discharge electrical efficiency and stability are, however, under active investigation.

Overall Thruster Performance

The overall thruster performance and power throttling data for the functional model thruster are presented in Table IV. Data were obtained over an input power range of 0.7-4.9 kW, at five different beam currents. The thruster was power-throttled about each of the beam current conditions by adjustment of the net-to-total voltage at a fixed ratio of 0.83. Overall thruster efficiencies vary from a peak of 0.72 at 4030 s specific impulse and 4.9 kW input power, down to 0.45 at 2290 s specific impulse and 0.7 kW input power. At the peak input power of 4.9 kW the discharge losses are 190 W/A at a total thruster propellant efficiency of 0.87. At the low power condition of 0.7 kW the discharge losses increase to approximately 280 W/A, while the total propellant efficiency drops to about 0.81.

Figures 12 displays the performance data of Table IV in a plot of thruster efficiency versus specific impulse for the NASA 30 cm thruster. Note in Fig. 12 that separate performance curves are obtained for each of the beam currents, with overall thruster efficiency increasing with increasing beam current for a given specific impulse. This is due to the reduction in discharge losses experienced with increasing beam current, as indicated in Fig. 13. The thruster efficiency begins to drop-off markedly at lower specific impulse and lower power levels as the fixed losses associated with the discharge and the neutralizer have a more pronounced impact on, and consume a larger fraction of, the thruster input power.

Figures 14 and 15 show the thrust and specific impulse versus thruster input power, respectively. In Fig. 14, a monotonic increase in thrust with input power is seen, varying from 28 mN at 0.7 kW to a peak of 178 mN at 4.9 kW. Figure 15 indicates roughly a 500 s specific impulse variation for a 1000 W input power variation at 3.0 A beam current, with somewhat higher sensitivities at the lower beam currents. Figure 16 compares the performance data obtained at the 1.1 A beam current condition identified in Table IV for two separate test segments, and good repeatability of performance is noted.

Power Throttling

Figure 17 shows the demonstrated power throttling range as a function of beam current, where power throttling was accomplished by maintaining a constant net-to-total voltage ratio of 0.83 (or equivalently, a constant ratio of screen-to-accelerator grid voltage of approximately 5:1) while varying the total voltage at fixed discharge power/fixed flow rate conditions. Where mission requirements dictate that the thruster be throttled, power throttling at constant thruster mass flow rates, and at a constant ratio of screen-to-accelerator grid voltage simplifies both the propellant management and power processor requirements. Fixed flow rate obviously alleviates propellant management flow control requirements, and a constant total voltage ratio allows for a common screen/accelerator power stage in the power processor.[18]

As indicated in Fig. 17 the demonstrated power throttling range at fixed flow rates is approximately 1.7:1 at 1.1 A beam current, and drops to approximately 1.35:1 at 3.0 A beam current. Note the lower end of the power throttling range at each beam current was constrained by the perveance limit. The upper end of the power throttling envelope was defined by a pre-specified maximum total voltage and thruster input power. Hence, these ranges are not necessarily the maximum envelope at each beam current, however the trend of reduced throttling range with increasing beam current is real.

Increasing the ion optics perveance would increase the power throttling range for a given beam current, however this will probably be at the expense of the minimum required accelerator grid voltage and discharge propellant efficiency. This is because there are two constraints on defining the operating accelerator grid voltage; the electron-backstreaming limit, and the perveance limit. Most modifications made to improve the ion optics perveance also tend to decrease the maximum obtainable

net-to-total voltage ratio. Hence, for a mission-defined specific impulse and input power which specifies the operating screen voltage, higher magnitude operating accelerator grid voltages may be required to accommodate large power throttling ranges, than would be necessary for a single-point operating condition.

At the fixed mass flow rate and discharge power conditions identified in Table IV, the beam current varied slightly as the total voltage was varied due to changes in the ion transparency of the optics. A maximum variation of 1.1:1 in beam current was experienced for a 1.6:1 variation in total voltage. This roll-off in beam current with decreasing total voltage accounts for a more rapid roll-off in thruster efficiency with decreasing specific impulse than that which might ordinarily be anticipated.

Thruster Lifetime Expectations

For the NASA 30 cm thruster, the erosion of the molybdenum accelerator grid due to charge-exchange processes is the dominant life limiting wear-mechanism. The accelerator grid is the minimum-life component for most of the thruster operational envelope, and all conditions for which the projected thruster lifetime is less than 10,000 hours.[12] As the erosion rate of the accelerator grid is strongly dependent on its voltage, it is advantageous to operate at the lowest possible magnitude of this voltage. Hence tests were conducted to identify minimum required accelerator grid voltages at each of the nominal operating conditions of Table IV, and these are shown in Table V.

Table V shows the accelerator grid voltage at which the on-set of electron-backstreaming begins to occur, and a minimum operating accelerator grid voltage which is approximately 20-30 volts greater magnitude and which is sufficient for steady-state operation. At a thruster input power of 2.40 kW, and a specific impulse of 3250 s, a minimum operating accelerator grid voltage of -150 volts is required. Figure 18 shows the maximum obtainable net-to-total voltage ratio, at the on-set of electron-backstreaming, as a function of beam current, for the conditions of Table V. As anticipated, the maximum obtainable ratio decreases with increasing beam current, going from approximately 0.92 at 0.8 A beam current, down to 0.89 at 2.3 A beam current.

Table VI compares the anticipated accelerator grid erosion rates, and on-ground and in-space thruster lifetimes for the conditions identified in Table V at the minimum operating accelerator grid voltages. The methodology used to estimate erosion rates and lifetimes is discussed in Appendix B. Note that except for on-ground testing of the thruster at 3.4 kW, lifetimes (both on-ground and in-space) greater than 10,000 h are anticipated for all thruster performance conditions of Table V. It is estimated that the thruster lifetime will be limited by erosion of the accelerator grid for all conditions identified in Table V, excepting for the lowest power condition where internal erosion of cathode potentials surfaces may dominate. At this condition, a lifetime of several tens-of-thousands of hours is anticipated.

SSTAR Mission

A preliminary mission plan for ion propulsion on-board the SSTAR platform calls for approximately 2.4 kW of power available to the 30 cm thruster. At this input power level, typical performance for the thruster is 95 mN thrust at 3250 s specific impulse, and an overall thruster efficiency of 0.63. Typical discharge operation is 0.90 propellant efficiency, at 200 W/A discharge losses. Total thruster propellant efficiency is 0.80. At these conditions, the thruster xenon consumption rate is 2.97 mg/s, or approximately 10.7 kilograms per thousand hours of operation.

The minimum-life component at these conditions is estimated to be the accelerator grid. At -150 volts accelerator grid voltage, a molybdenum mass efflux rate from the thruster of 2.9 grams per thousand hours of operation is anticipated in-space, with a somewhat higher mass efflux rate expected during ground-testing depending upon the pumping speed of the test facility. This in-space mass efflux rate is believed to be consistent with an accelerator grid lifetime of $\rangle$ 24,000 h. Thruster lifetime estimates based on erosion of cathode-potential surfaces in the thruster discharge yield a factor of 2 greater lifetime, due to the relatively low operating discharge voltage (28-29 volts) and ion current density (2.9 mA/cm^2) at this operating condition.

Development Activities

Vibration Testing

The thruster has undergone a series of low level sine sweep vibration tests conducted at the NASA Lewis Research Center's Structural Dynamics Laboratory, detailed results of which can be found in reference 20.

The objective of these tests was to investigate the general behavior of the thruster to evaluate its vibration characteristics and to provide information on its vibration strength. The tests consisted of applying an excitation frequency from 5 Hz to 2 kHz at a one octave per minute sweep rate at amplitudes of 0.5 and 1.0 g through the three orthogonal axes of the thruster. The intention was to determine the natural frequencies of the thruster and obtain information regarding the non-linearity of response with increased excitation level. A total of 19 accelerometers were installed on the thruster to measure local structural response at various locations.

No damage to the thruster was incurred during the conduct of the test, and no deterioration was identified during subsequent disassembly. However the test did indicate areas for design modification and improvement including the neutralizer assembly and the gimbal pads. Additional tests at higher amplitudes will be required to fully validate the structural integrity of the design.

Component Life Testing

A test program is on-going to develop and validate hollow cathode technology for the space station Freedom plasma contactor program.[22] Much of the technology, and cathode components, for the thruster are common with the plasma contactor including the cathode insert, the neutralizer, and heater subassemblies. Hence, much of the life test and performance data derived from the hollow cathode contactor activity is directly transportable to the engineering model thruster development. These activities include hollow cathode and heater life testing and validation[23,24], definition and validation of contamination control protocols and procedures implemented in the propellant management system, definition and verification of conditions for cathode ignition, and development of cathode storage, handling and activation requirements.

Documentation

A CAD drawing package for the functional model thruster is being developed, using CADAM.[25] The drawing package consists of approximately 100 drawings and includes all thruster subsystems and associated fabrication, assembly, and inspection procedures. The drawing package will be provided to industry as part of the ion thruster technology transfer program. Additionally, procurement specifications for critical cathode components such as the insert are being developed. These specifications include definition of all critical aspects of the chemical and physical makeup to insure procurement of a reliable product for flight.

Additional activities to develop and validate a 30 cm engineering model ion thruster include:

define and verify conditions for discharge chamber and neutralizer cathode ignition;

initiate detailed characterizations of thruster interfaces including EMC and plume surveys;

initiate wear testing to verify thruster design and lifetime expectations, and;

initiate thruster/breadboard power processor integration testing.

Concluding Remarks

A 30 cm diameter xenon ion thruster is under development at NASA to provide an ion propulsion option for auxiliary and primary propulsion on missions of national interest. Under this program the ion thruster is being brought to engineering model development status. Goals of the development effort include a thruster mass of 7 kg, and an operating power envelope of 0.5 to 5.0 kW. The present thruster hardware under test is at a functional model level of maturity. The thruster incorporates major innovations in structural design, materials, and fabrication techniques compared to those employed in conventional ion thrusters.

Performance data for the thruster were obtained over a 0.7-4.9 kW power envelope to verify the performance of the aluminum, partial-conic discharge chamber design and evaluate stability; quantify overall thruster performance, and; evaluate power throttling at fixed mass flow rate conditions.

The functional model thruster performance stability, as measured by the specific impulse and efficiency sensitivities to variations in cathode flow rate, compares favorably to other thrusters. Additional tests to improve discharge electrical efficiency and stability are, however, under active investigation. Overall thruster efficiencies vary from a peak of 0.72 at 4030 s specific impulse and 4.9 kW input power, down to 0.45 at 2290 s specific impulse and 0.7 kW input power. At the peak input power of 4.9 kW the discharge losses are 190 W/A at a total thruster propellant efficiency of 0.87. At the low power condition of 0.7 kW the discharge losses increase to approximately 280 W/A, while the total propellant efficiency drops to about 0.81. The demonstrated power throttling range via

total accelerator voltage variation at fixed flow rates is approximately 1.7:1 at 1.1 A beam current, and drops down to approximately 1.35:1 at 3.0 A beam current.

For the NASA 30 cm thruster, the erosion of the molybdenum accelerator grid due to charge-exchange processes is believed to be the dominant life limiting wear-mechanism. However, in-space lifetimes greater than 10,000 h are anticipated for all thruster performance conditions.

The SSTAR mission plan calls for approximately 2.4 kW of power available to the 30 cm thruster. At this input power level, typical performance for the thruster is 95 mN thrust at 3250 s specific impulse, and an overall thruster efficiency of 0.63. Total thruster propellant efficiency is 0.80. At these conditions, the thruster xenon consumption rate is 2.97 mg/s, or approximately 10.7 kilograms per thousand hours of operation. At -150 volts accelerator grid voltage, a molybdenum mass efflux rate from the thruster of 2.9 grams per thousand hours of operation is anticipated in-space, with a somewhat higher mass efflux rate expected during ground-testing. This in-space mass efflux rate is believed to be consistent with an accelerator grid lifetime of $\rangle$ 24,000 h.

Additional on-going activities to bring the thruster to engineering model development status include vibration testing, component life testing, and generation of a CAD drawing package. As these activities are completed, efforts to evaluate thruster interfaces, verify thruster lifetimes, and integrate the thruster with a power processor will be initiated.

Acknowledgements

The authors would like to express their appreciation to Eli Green, George Jacynycz, Craig Nelson, and Eugene Pleban for test support, thruster assembly and suggestions in design.

References

[1]Groh, K., et. al., "Development Status of the RIT Ion Engines, " AIAA Paper No. 90-2671, July 1990.

[2]Fearn, D.G., "The Proposed Demonstration of the UK-10 Ion Propulsion System on ESA's SAT-2 Spacecraft," IEPC Paper No. 88-031, October 1988.

[3]Kajiwara, K. and Katada, M., "Test Facilities for the ETS-VI Ion Engine System," AIAA Paper No. 90-2656, July 1990.

[4]Patterson, M.J. and Verhey, T.R., "5kW Xenon Ion Thruster Lifetest," AIAA Paper No., 90-2543, July 1990.

[5]Rawlin, V.K., "Internal Erosion Rates of a 10-kW Xenon Ion Thruster," AIAA Paper No. 88-2192, July 1988.

[6]Patterson, M.J. and Rawlin, V.K., "Performance of 10-kW Class Xenon Ion Thrusters," AIAA Paper No. 88-2914, July 1988.

[7]Patterson, M.J. and Williams, G.J. Jr., "Krypton Ion Thruster Performance," AIAA Paper No. 92-3144, July 1992.

[8]Sovey, J.S., "Improved Ion Containment Using a Ring-Cusp Ion Thruster," *Journal of Spacecraft and Rockets*, Vol. 21, Sept.-Oct. 1984, pp. 488-495.

[9]Patterson, M.J. and Rawlin, V.K., "Derated Ion Thruster Design Issues," IEPC Paper No. 91-150, October 1991.

[10]Rawlin, V.K., "Characterization of Ion Accelerating Systems on NASA's Ion Thrusters," AIAA Paper No. 92-3827, July 1992.

[11]Patterson, M.J. and Mohajeri, K., "Neutralizer Optimization," IEPC Paper No. 91-151, October 1991.

[12]Patterson, M.J., "Low-Isp Derated Ion Thruster Operation," AIAA Paper No. 92-3203, July 1992.

[13]Verhey, T.R. and Patterson, M.J., "Microanalysis of Extended-Test Xenon Hollow Cathodes," AIAA Paper No. 91-2123, June 1991.

[14]Sarver-Verhey, T.R., "Extended Testing of Xenon Ion Thruster Hollow Cathodes," AIAA Paper No. 92-3204, July 1992.

[15]Patterson, M.J. and Foster, J.E., "Performance and Optimization of a "Derated" Ion Thruster for Auxiliary Propulsion," AIAA Paper No. 91-2350, June 1991.

[16]Rawlin, V.K. and Majcher, G., "Mass Comparisons of Electric Propulsion Systems for NSSK of Geosynchronous Spacecraft," AIAA Paper No. 91-2347, June 1991.

[17]30-Centimeter Ion Thruster Subsystem Design Manual," NASA TM-79191, June 1979.

[18]Rawlin, V.K., Pinero, L., and Hamley, J., "Simplified Power Processing for Inert Gas Ion Thrusters," AIAA Paper No. 93-2397, June 1993.

[19]Personal communication, Mantenieks, M.A., NASA-Lewis Research Center, May 1993.

[20]Patterson, M.J., Haag, T.W., and Williams, G.J., "Derated Ion Thruster Development Status," AIAA Paper No. 93-2225, June 1993.

[21]Beattie, J.R. and Matossian, J.N., "High Power Ion Thruster Technology," NAS 3-25553 Final Report, pp. E3, June 1991.

[22]Patterson, M.J., et al., "Plasma Contactor Technology

for Space Station Freedom," AIAA Paper No. 93-2228, June 1993.

[23]Sarver-Verhey, T., "Extended Test of a Xenon Hollow Cathode for a Space Plasma Contactor," IEPC Paper No. 93-020, September 1993.

[24]Soulas, G., "Hollow Cathode Heater Development for the Space Station Freedom Plasma Contactor," IEPC Paper No. 93-042, September 1993.

[25]CADAM is a registered trademark of International Business Machines.

Appendix A

Performance Calculations -

The following equations and assumptions were used in the calculations of thruster performance:

- Thrust, in mN -

$$F = \gamma \left(2\frac{m}{q}\right)^{1/2} J_b \left(V_b\right)^{1/2}. \qquad (A1)$$

The total thrust-loss correction factor is given by

$$\gamma = \alpha F_t. \qquad (A2)$$

The correction factor for doubly-charged ions is calculated from the equation

$$\alpha = \frac{\left(1 + 0.7071 \frac{I^{++}}{I^{+}}\right)}{\left(1 + \frac{I^{++}}{I^{+}}\right)}. \qquad (A3)$$

As a spectrometer probe was not available during this investigation, beam-centerline current data for a similar type thruster operating on xenon, correlated to discharge chamber propellant utilization efficiency, was used for this analyses.[A1] The use of this centerline data is expected to yield a worst-case correction factor. The thrust-loss correction factor for off-axis vectoring was calculated from the polynomial equation

$$F_t = \Delta Ft - 0.1470 + 0.8440(R) - 2.0675(R)^2 + 2.3661(R)^3 - 1.0167(R)^4, \qquad (A4)$$

obtained from a curve fit of experimental data of Danilowicz, et. al..[A2] In equation A4, R is the ratio of net-to-total accelerating voltage. An additional term ΔF_t is included as a normalization constant to take into account thrust-loss dependency on ion optics electrode geometry. This term is a product of three correction factors, one each for the accelerator-to-screen grid aperture diameter ratio, accelerator grid thickness-to-screen grid diameter ratio, and the grid gap-to-screen grid aperture diameter ratio. The values of these correction factors were obtained from curves fits of experimental data of Kaufman.[A3]

The beam voltage in equation A1 is given by

$$V_b = V_s + V_d - |V_g|. \qquad (A5)$$

Note that the output of the screen power supply is tied to negative side of the discharge power supply in the present test configuration.

- Specific impulse, in seconds -

$$I_{sp} = \eta_u \gamma \left(2qV_b/m\right)^{1/2} (1/g). \qquad (A6)$$

The total propellant utilization efficiency is calculated from the equation

$$\eta_u = J_b/M_0. \qquad (A7)$$

The total propellant flow rate is the sum of the propellant flow rates through the main plenum, the discharge cathode, and the neutralizer cathode, and an additional term for propellant flow ingested from the facility back into the thruster discharge chamber. The ingested flow from the facility in equivalent amperes can be approximated by the equation[A4]

$$M_i = 2x10^4 T_{pc} A_{oaa}/(M)^{1/2}. \qquad (A8)$$

- Input power -

$$P_{inpt} = (V_s J_s) + (V_d J_d) + (J_{nk} V_{nk}) + (J_a |V_a|). \qquad (A9)$$

- Total thruster efficiency -

$$\eta_t = \frac{F I_{sp} g}{2 P_{inpt}}. \qquad (A10)$$

References

[A1]Rawlin, V.K., "Operation of the J-Series Thruster

Using Inert Gas," NASA TM-82977, November 1982.

[A2]Danilowicz, R.L., et. al., "Measurement of Beam Divergence of 30-Centimeter Dished Grids," AIAA Paper No. 73-1051, October 1973.

[A3]Kaufman, H.R., "Accelerator-System Solutions for Electron Bombardment Ion Sources," March 1975.

[A4]Sovey, J.S., "Improved Ion Containment Using a Ring-Cusp Ion Thruster," NASA TM-82990, November 1982.

Appendix B

Lifetime Calculations -

The following equations and assumptions were used in the calculation of thruster lifetimes:

Overall thruster lifetimes were determined from the minimum estimated lifetime of 2 critical components which were the accelerator grid, and cathode-potential surfaces in the discharge chamber. The wear-mechanism associated with the accelerator grid is assumed to be erosion by charge-exchange ions, impacting both thruster lifetime and spacecraft contamination via metal efflux. Over a prolonged period of time the sputtering of the downstream surface of the accelerator grid can lead to its structural failure.

Under normal operating conditions most of the accelerator impingement current is due to charge-exchange ion impingement, and one can therefore assume that the measured accelerator current is equal to the charge-exchange ion current since direct ion impingement currents are expected to be very small. Additionally, for purposes of calculating sputter yields, it can be assumed that the incident energy of the charge-exchange ions can be approximated by the accelerator grid voltage. Under these conditions, it is possible to obtain reasonable correlation of accelerator grid mass loss rates to the product of the accelerator grid impingement current and the appropriate sputter yield.[B1] However, due to uncertainties associated with sputter yields, an alternative approach was used. A simple correlation of the ratio of accelerator grid mass loss rate-to-impingement current with accelerator grid voltage was obtained for four separate xenon ion thruster wear tests.[B2-B5] Using a curve-fit of these data for grid voltages $\rangle$ 200 V, and a linear extrapolation to zero for voltages $\leq$ 200 V, results in conservative mass loss estimates compared to that which would obtained from sputter yields. These data are shown in Figure B1.

Under most test conditions of the thruster, a significant fraction of the accelerator impingement current was due to 'facility-enhanced' charge-exchange processes. That is, under these conditions a dominant term in the volume ion production of charge-exchange ions was due to the neutral density contribution from residual propellant atoms in the facility. To account for this affect so as to obtain an estimated mass loss rate for in-space conditions listed in Table VI it was assumed that the space-equivalent accelerator drain current would be equal to 0.25% of the beam ion current. This value of impingement current is consistent with ground test data for both mercury and xenon propellant under conditions of low background pressures and comparable ion optics geometries. Mass loss rate estimates were then obtained for all thruster operating conditions by using the accelerator grid operating voltages and associated impingement currents as inputs to the curve of Fig. B1.

The erosion patterns due to charge-exchange processes are fairly complex, and hence while estimates of mass loss rates may be reasonably accurate, it is difficult to convert these values into accelerator grid lifetimes with certainty. The method employed here was based on the examination of several post-test accelerator grids of various geometries to identify a common definition of end-of-life, and correlation of same to the total mass lost. A loss of a total of 70 grams, corresponding to roughly ~27% of the effective accelerator grid mass, was chosen as end-of-life. This value is probably conservative, as at this condition, the accelerator electrode is still structurally viable. This is lower than the 35% mass loss, end-of-life estimate of Reference B3.

The life-limiting mechanism associated with the screen grid is assumed to be sputter erosion of its surface by discharge ions, eventually leading to structural failure of this component. The internal erosion rate of the screen grid is proportional to

$$R_{scrn} \propto \frac{j^{+}Y(E) + \frac{j^{++}}{2}Y(2E)}{\Phi_s} . \qquad (B1)$$

From equation B1, the erosion rate is given by the product of the ion current density impinging on the screen grid and the physical sputter yield at the incident ion energy, with the doubly-charged ions being accelerated by

the sheath drop to twice the energy of the singly-charged ions.

Data for low energy sputtering (⟨ 100 eV) for xenon ions on molybdenum and other refractory metals is virtually non-existent. Hence a simple analysis was employed[B6] to estimate sputter yields in this energy range, the results of which are shown in Figure B3 of reference B1.

The erosion rates calculated from equation B1 were converted to an absolute lifetime by normalizing the values to that obtained from a high-power wear test of a 30 cm xenon ion thruster[B2], and defining end-of-life to be at a condition where the centerline screen grid erosion was sufficient to reduce the grid to half its original thickness.

References

[B1]Patterson, M.J., "Low-Isp Derated Ion Thruster Operation," AIAA Paper No. 92-3203, July 1992.

[B2]Patterson, M.J., and Verhey, T.R., "5kW Xenon Ion Thruster Lifetest," AIAA Paper No. 90-2543, July 1990.

[B3]Kitamura, S., Miyazaki, K., and Hayakawa, Y., "1000 Hour Test of 14 cm Diameter Ring-Cusp Xenon Ion Thruster," AIAA Paper No. 90-2542, July 1990.

[B4]Kitamura, S., Miyazaki, K., and Hayakawa, Y., "Cyclic Test of a 14 cm Diameter Ring-Cusp Xenon Ion Thruster," AIAA Paper No. 92-3146, July 1992.

[B5]Beattie, J.R., and Matossian, J.N., "Xenon Ion Propulsion for Stationkeeping and Orbit Raising," AIAA Paper No. 88-052, October 1988.

[B6]Patterson, M.J., and Foster, J.E., "Performance and Optimization of a 'Derated' Ion Thruster for Auxiliary Propulsion," AIAA Paper No. 91-2350, June 1991.

Table I Functional Model Thruster Design Objectives

propellant	xenon
size	30 cm {28 cm beam diameter}
mass	≈ 7 kg
input power	0.5 - 5.0 kW
lifetime	≥ 10,000 h

Table II Ion Optics Electrode Designs

electrode design	electrodes	
attribute	screen	accelerator
electrode thickness, mm	0.38	0.38
hole diameter, mm	1.91	1.14
open-area-fraction	0.67	0.24

Table III Performance Sensitivities to Cathode Flow Rate Variation

input power, kW	beam current, A	$\partial V_d/\partial m_c$, V/sccm	$\partial J_b/\partial m_c$, A/sccm	$\partial I_{sp}/\partial m_c$, s/sccm	$\partial \eta_t/\partial m_c$, %/sccm
2.43	1.8	-12.0	-0.46	-863	-14.1
1.56	1.1	-5.58	-0.11	-452	-6.36
0.86	0.8	-8.12	-0.08	-395	-3.90
0.53	0.8	-6.97	-0.07	-283	-3.09

Table IV NASA 30 cm Thruster Performance and Power Throttling Data

Beam Current, A	Isp, s	Input Power, kW	Thrust, mN	Efficiency	Mass Flow Rate, mg/s	Screen Voltage, V	Accel Voltage, V	notes
3.0	4030	4.88	178	0.72	4.50	1371	276	-
3.0	3740	4.34	165	0.70	4.50	1222	249	nominal cond't.
3.0	3470	3.88	154	0.68	4.50	1090	225	-
2.4	3790	3.86	142	0.69	3.83	1370	283	-
2.3	3510	3.43	132	0.66	3.83	1228	246	nominal cond't.
2.3	3250	3.05	122	0.64	3.83	1091	227	-
2.2	2950	2.67	111	0.60	3.83	961	199	-
1.9	3880	3.03	110	0.69	2.88	1365	271	-
1.8	3610	2.70	102	0.67	2.88	1224	254	-
1.8	3370	2.43	95	0.65	2.88	1094	225	nominal cond't.
1.8	3110	2.16	88	0.62	2.87	965	201	-
1.7	2820	1.89	80	0.58	2.87	842	169	-
1.1	3860	1.90	67	0.66	1.76	1372	280	-
1.1	3630	1.73	62	0.65	1.76	1227	245	-
1.1	3400	1.56	59	0.63	1.76	1093	222	nominal cond't.
1.1	3150	1.40	54	0.60	1.76	963	204	-
1.1	2920	1.26	50	0.58	1.76	843	169	-
1.1	2680	1.12	46	0.54	1.76	730	149	-
0.8	3180	1.07	39	0.57	1.25	990	250	-
0.8	2940	0.96	36	0.54	1.25	864	217	nominal cond't.
0.8	2710	0.86	33	0.51	1.25	745	185	-
0.8	2490	0.77	30	0.48	1.24	629	156	-
0.7	2290	0.70	28	0.45	1.23	552	133	-

Table V Minimum Accelerator Grid Voltages

Beam Current, A	Isp, S	Input Power, kW	Thrust, mN	Efficiency	Specified Screen Voltage, V	Back-streaming Accel Voltage[1], V	Min. Operating Accel Voltage[2], V
2.3	3480	3.41	131	0.66	1225	-150	-170
1.8	3250	2.40	95	0.63	1089	-120	-150
1.1	3360	1.56	59	0.62	1089	-100	-120
0.8	2900	0.96	36	0.54	860	-70	-90

[1]Voltage at which on-set of electron-backstreaming begins to occur.
[2]Voltage at which thruster operated in a stable condition for extended periods.

Table VI Anticipated Accelerator Grid Erosion Rates and Thruster Lifetimes

Thruster Input Power, kW	Measured Accel Impinge-ment Current, mA	Minimum Operating Accel Grid Voltage, V	On-ground Accel Grid Mass Loss Rate,[1] g/kh	On-ground Thruster Lifetime,[2] h	In-space Accel Grid Mass Loss Rate,[1] g/kh	In-space Thruster Lifetime,[3] h
3.41	14.8	-170	10.8	6,500	4.18	16,700
2.40	10.4	-150	6.68	10,500	2.89	24,200
1.56	4.0	-120	2.05	⟩⟩20,000	1.41	⟩⟩20,000
0.96	1.9	-90	0.73	⟩⟩20,000	0.73	⟩⟩20,000

[1]Mass loss rate estimates based on correlation of xenon ion thruster lifetest results, and is more conservative than that derived from published sputter yield data.
[2]70 gram total mass loss criteria for accelerator grid end-of-life; 110,000 ℓ/s xenon pumping speed facility.
[3]70 gram total mass loss criteria for accelerator grid end-of-life.

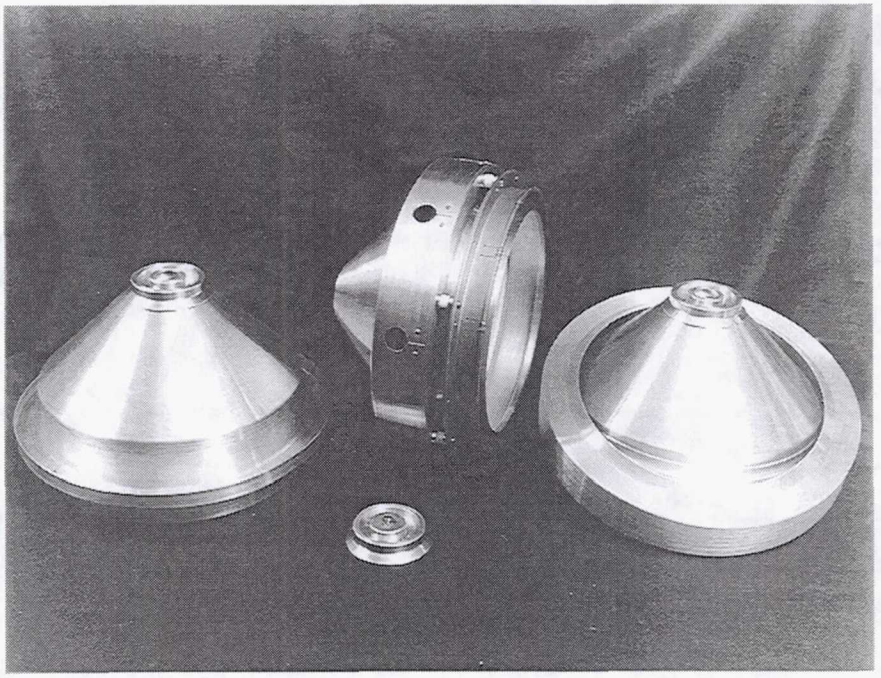

NASA C# 92-635

Fig. 1 Discharge chambers for functional model thrusters.

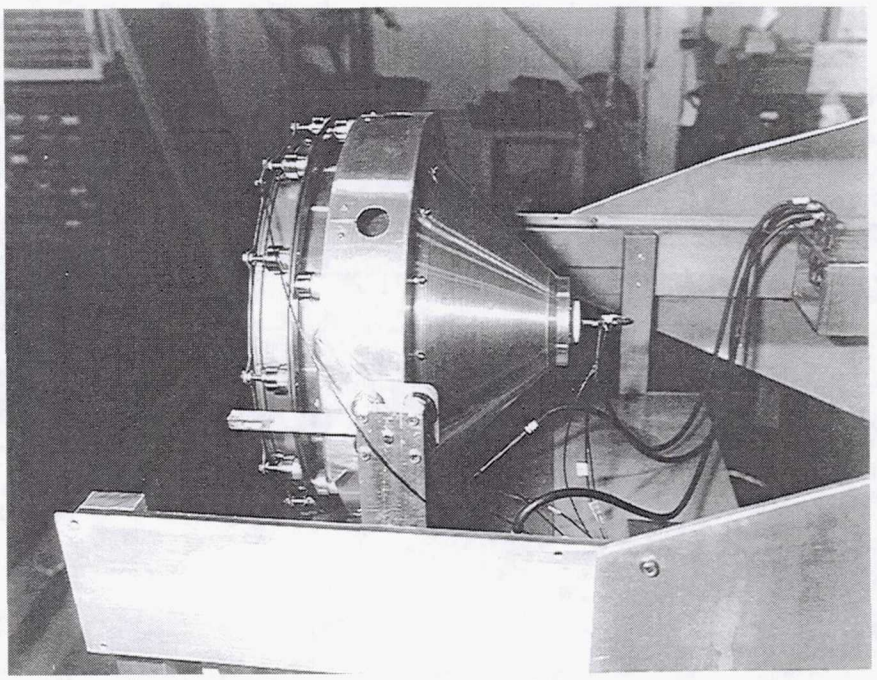

Fig. 2 Functional model thruster on test stand.

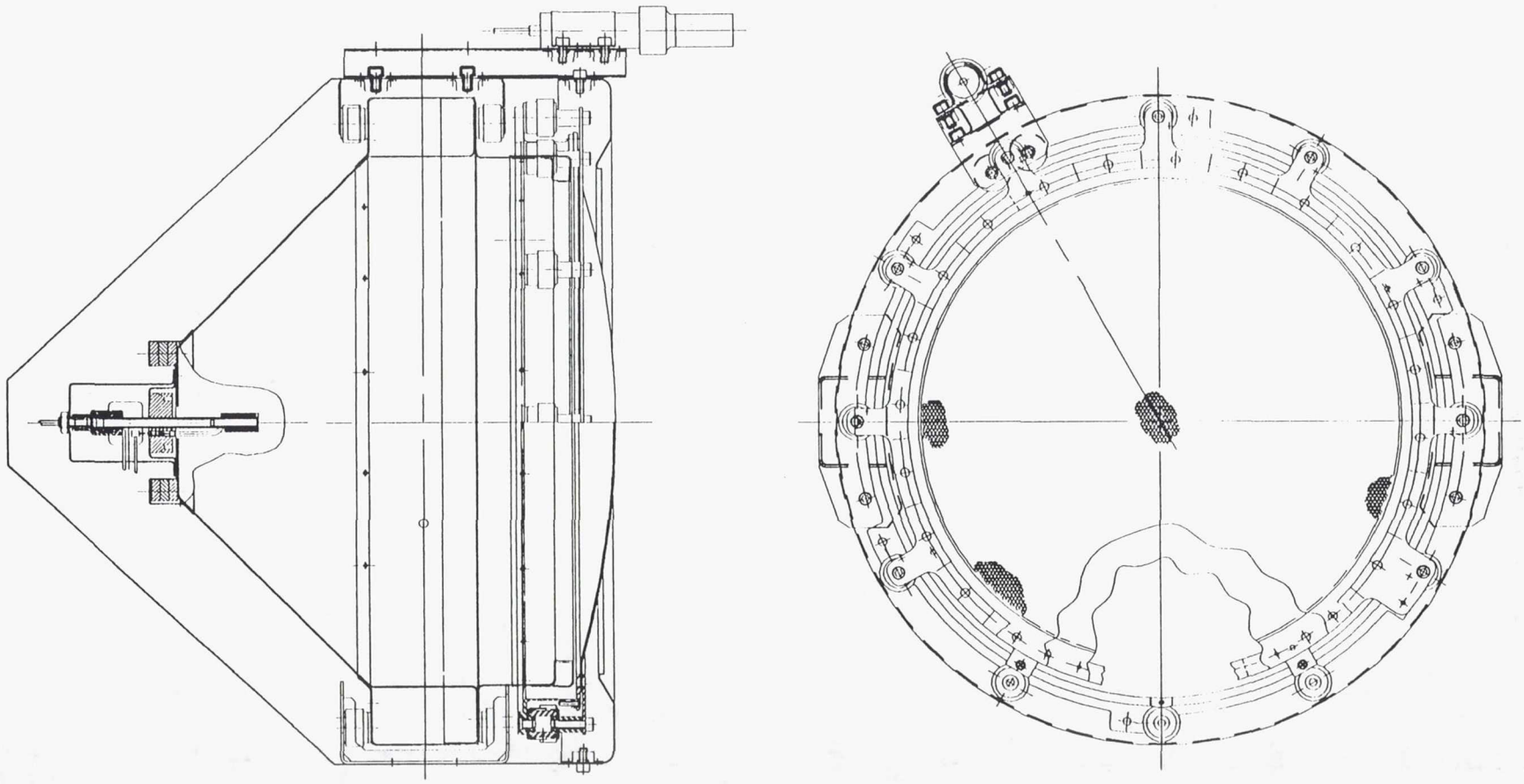

Fig. 3 NASA 30 cm diameter engineering model thruster.

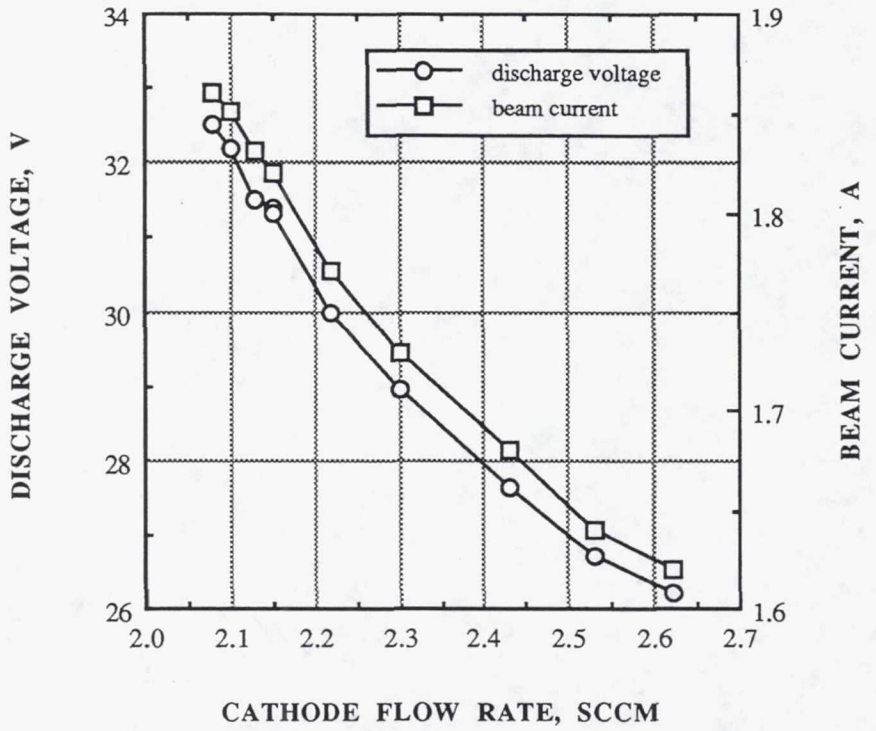

Fig. 4 Sensitivity of discharge voltage and beam current to variations in cathode flow rate; 2.4 kW condition.

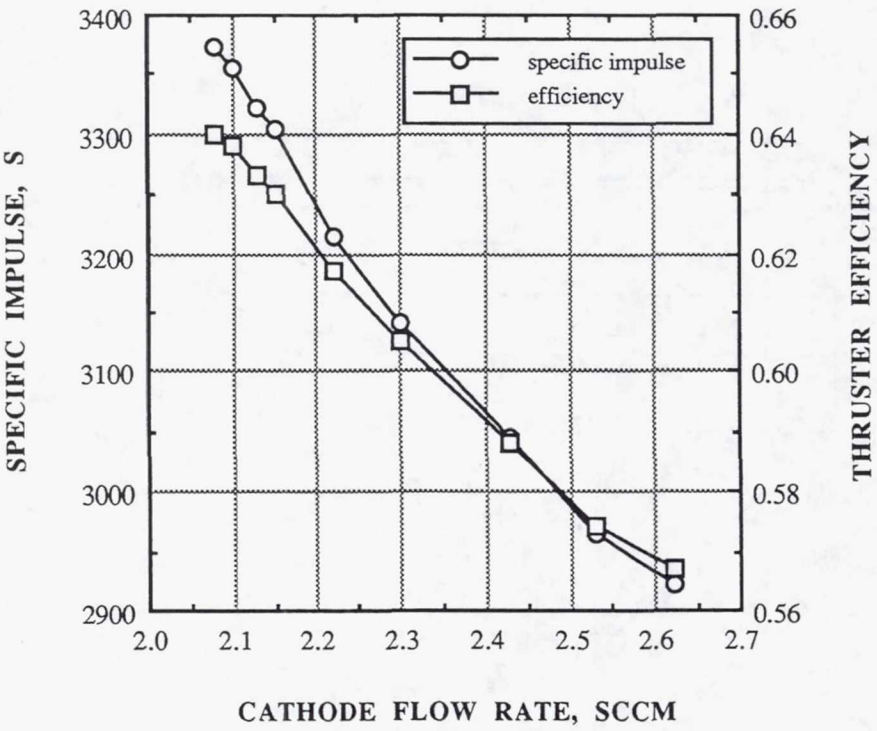

Fig. 5 Sensitivity of specific impulse and efficiency to variations in cathode flow rate; 2.4 kW condition.

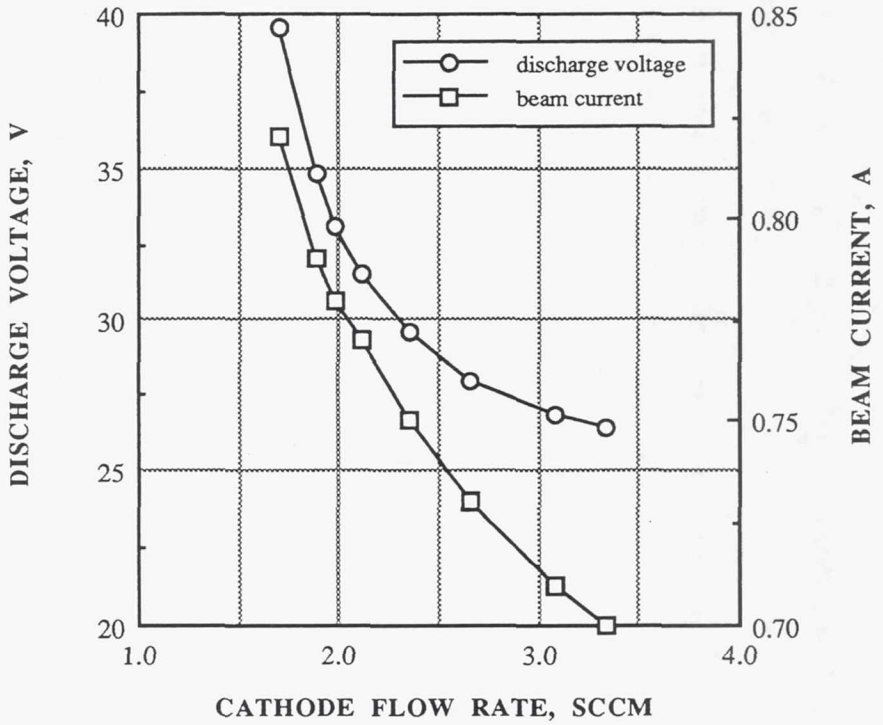

Fig. 6 Sensitivity of discharge voltage and beam current to variations in cathode flow rate; 0.53 kW condition.

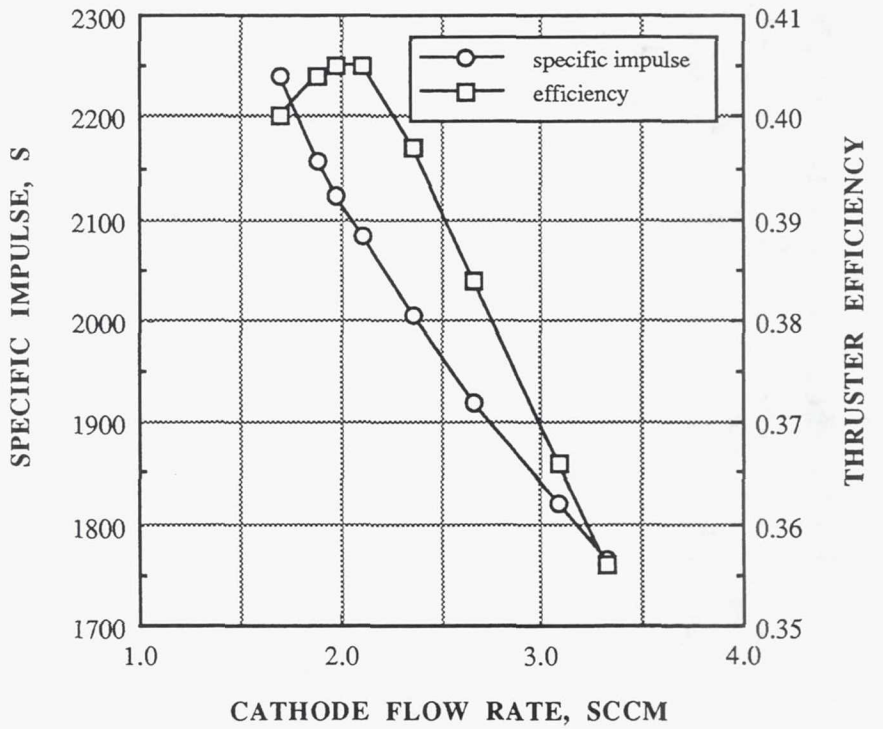

Fig. 7 Sensitivity of specific impulse and efficiency to variations in cathode flow rate; 0.53 kW condition.

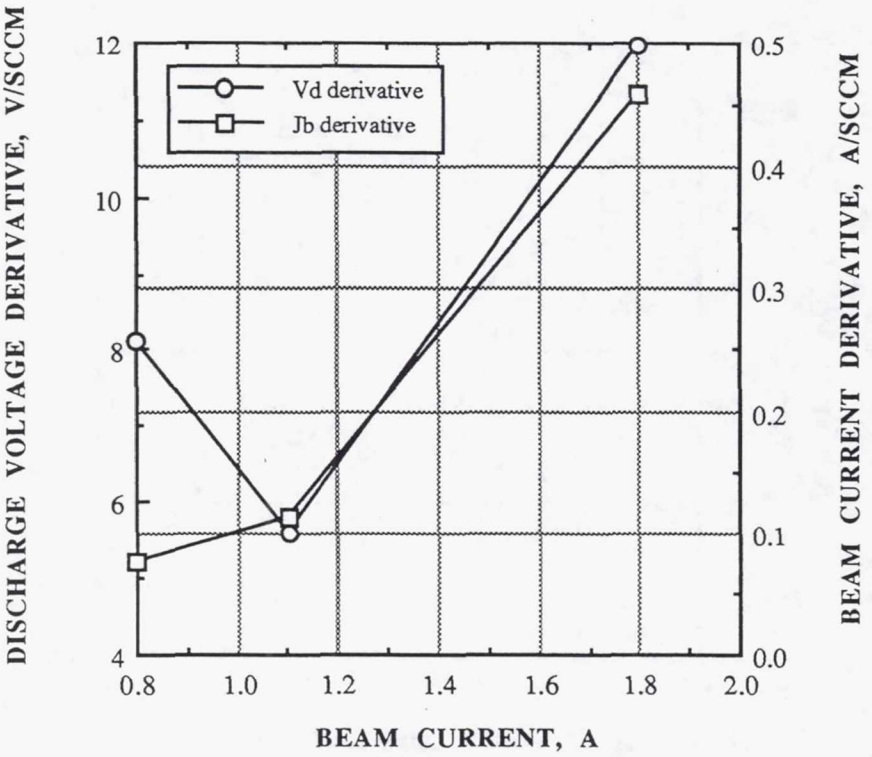

Fig. 8 Discharge voltage and beam current derivatives as a function of beam current.

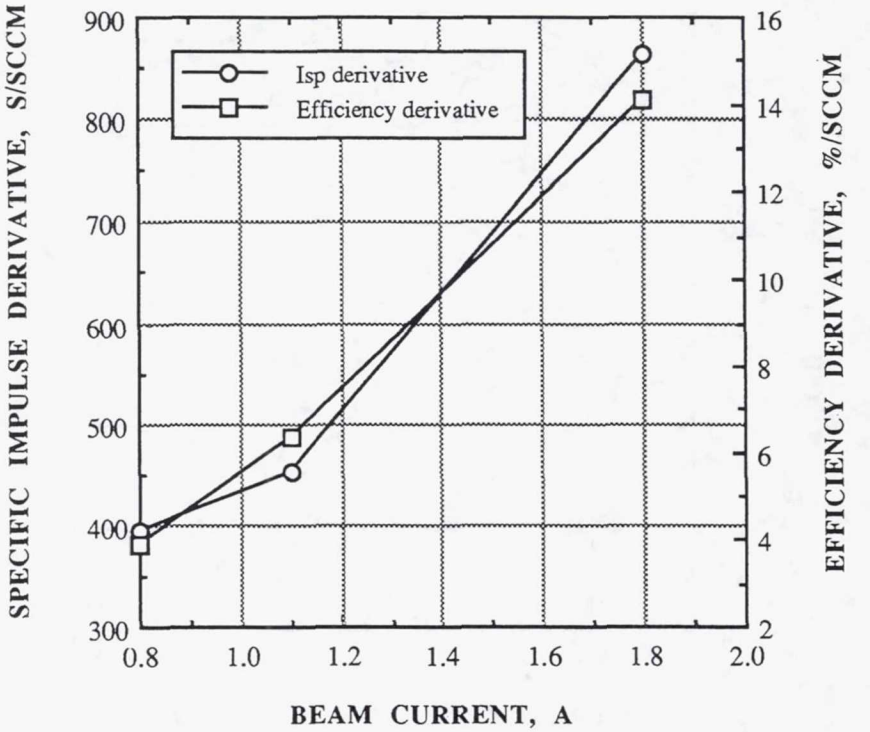

Fig. 9 Specific impulse and efficiency derivatives as a function of beam current.

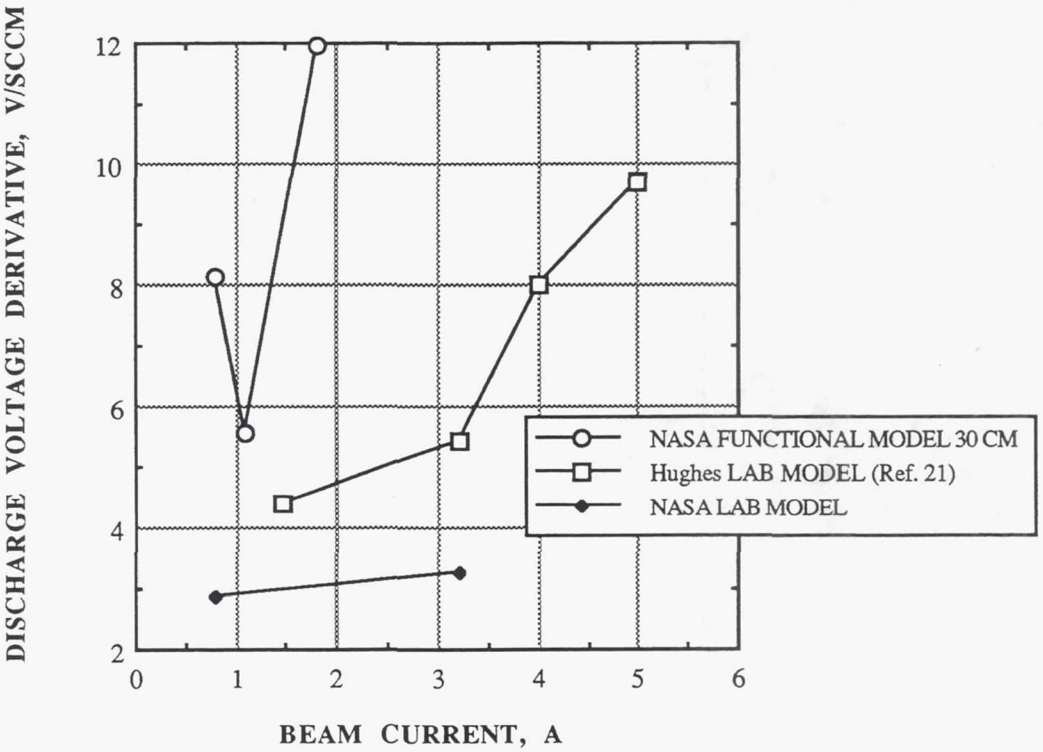

Fig. 10 Comparison of discharge voltage derivatives as a function of beam current.

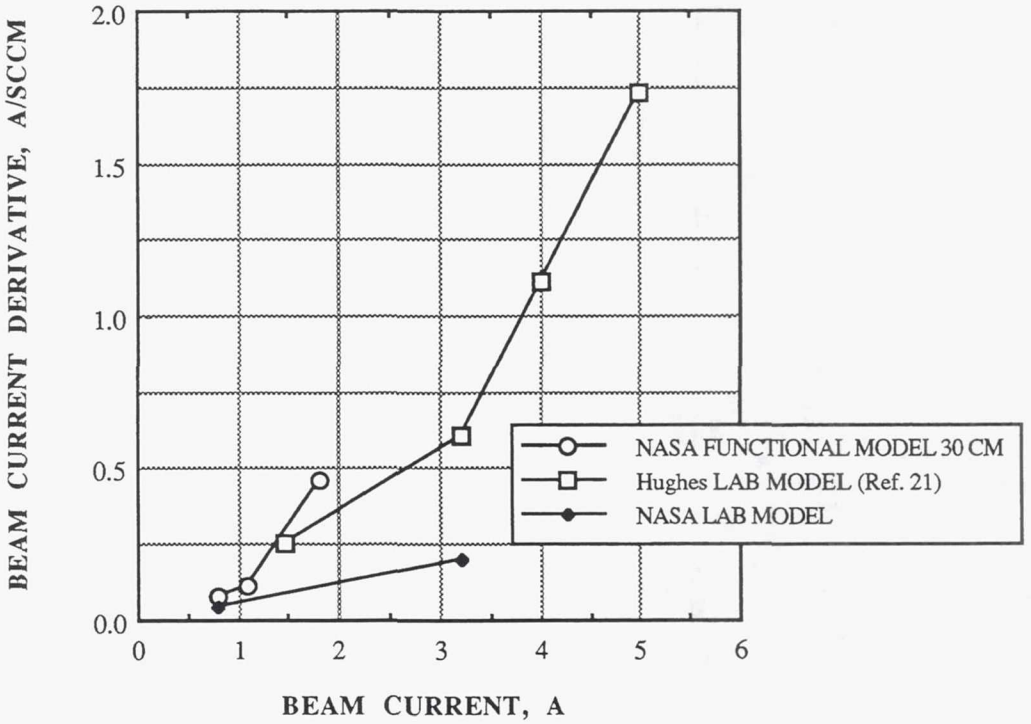

Fig. 11 Comparison of beam current derivatives as a function of beam current.

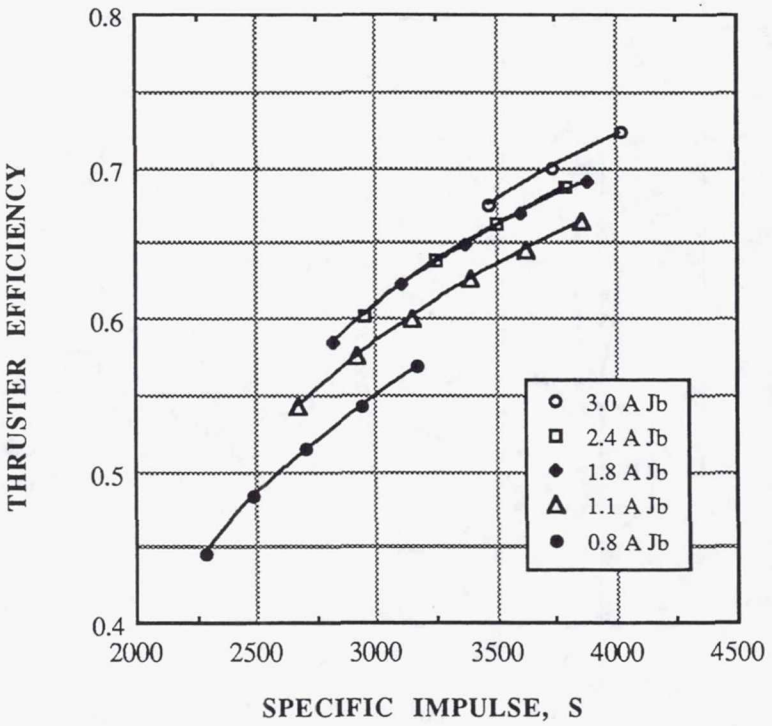

Fig. 12 Thruster efficiency versus specific impulse, for various beam currents.

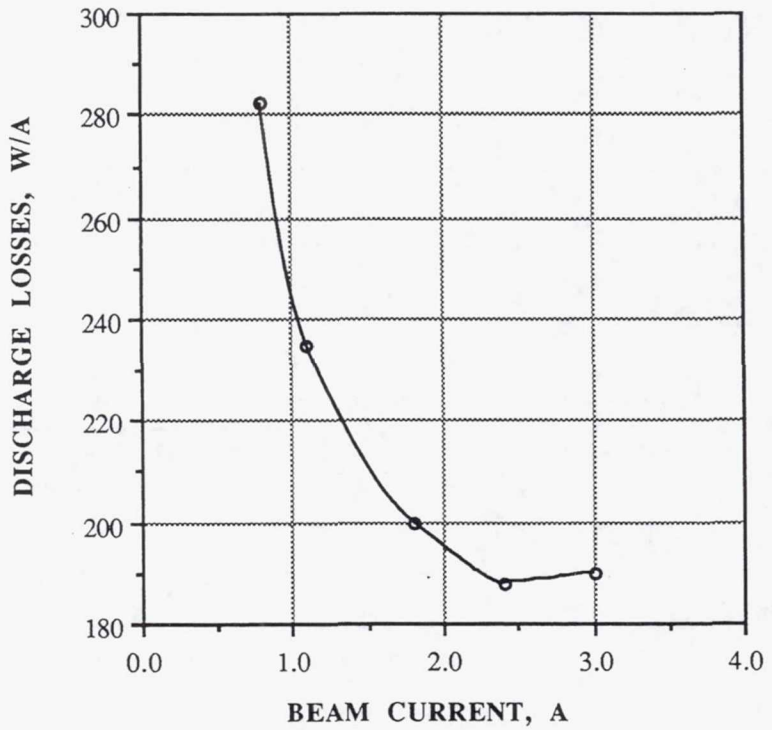

Fig. 13 Variation in discharge losses with beam current.

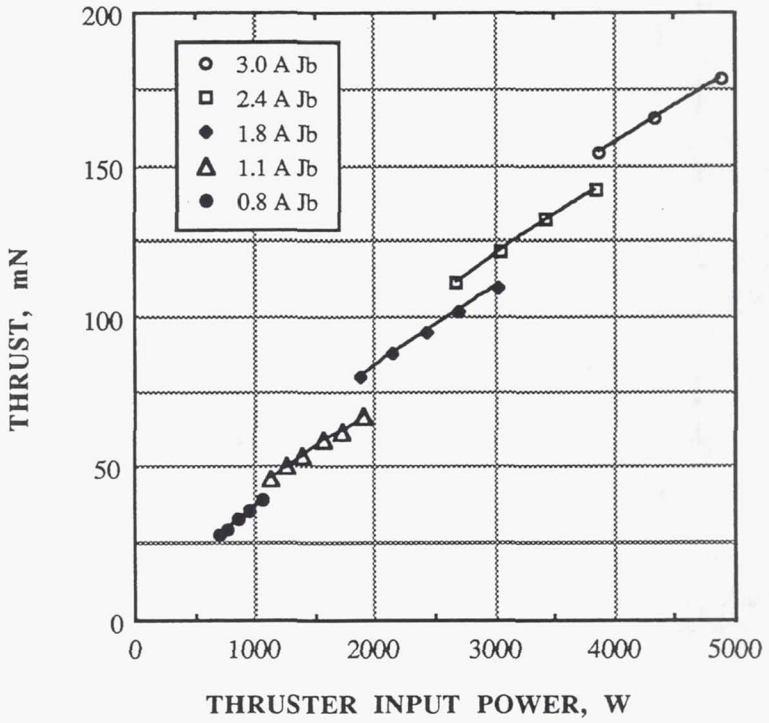

Fig. 14 Thrust versus thruster input power, for various beam currents.

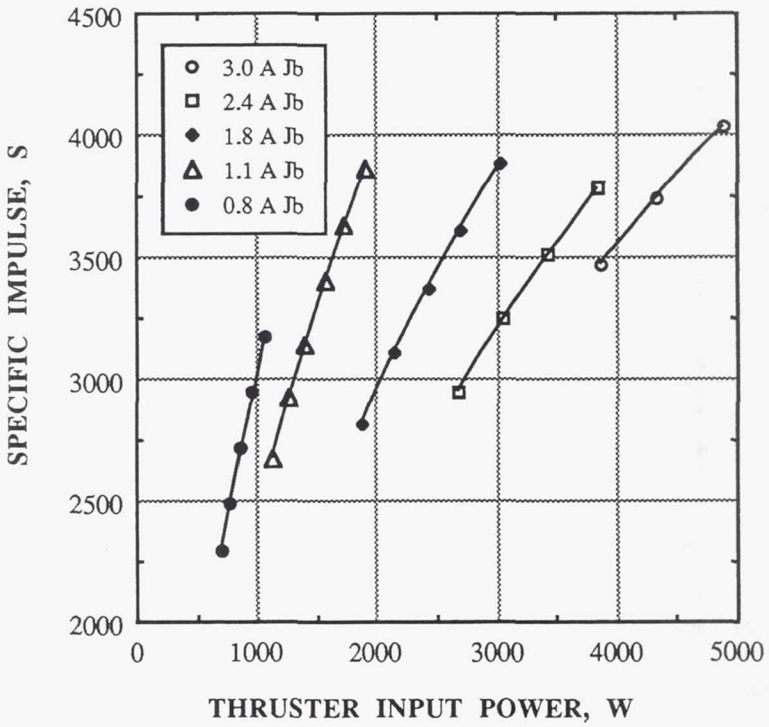

Fig. 15 Specific impulse versus thruster input power, for various beam currents.

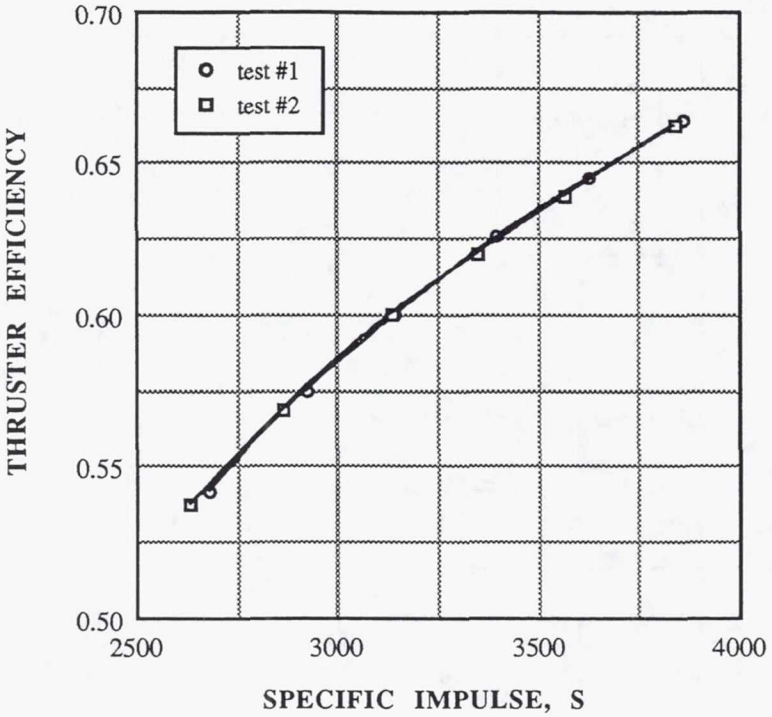

Fig. 16 Thruster performance comparison; 1.1 A beam current.

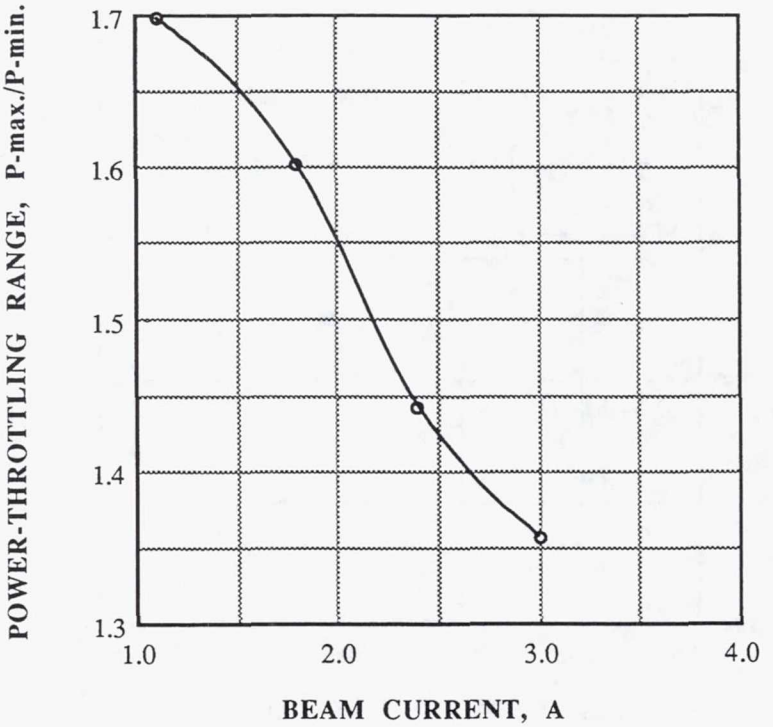

Fig. 17 Power-throttling range versus beam current.

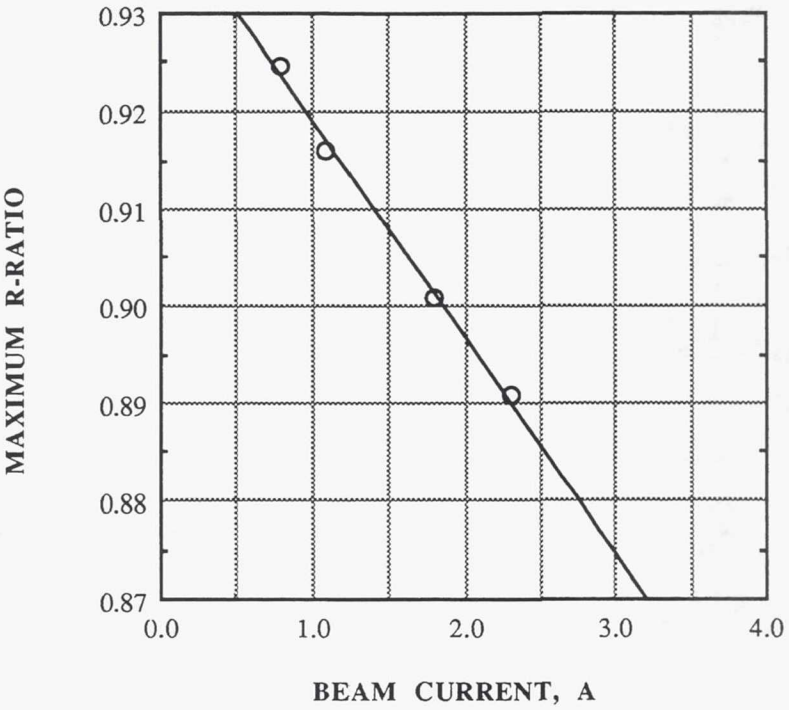

Fig. 18 Ion optics performance.

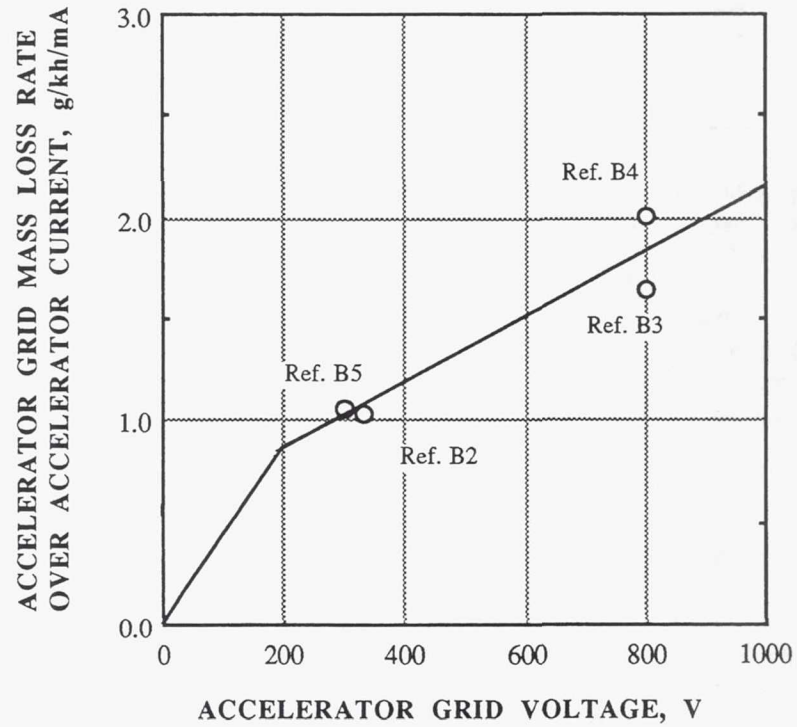

Fig. B1 Accelerator grid mass loss rate correlation.

REPORT DOCUMENTATION PAGE

Form Approved
OMB No. 0704-0188

1. AGENCY USE ONLY (*Leave blank*)	2. REPORT DATE	3. REPORT TYPE AND DATES COVERED
	December 1993	Technical Memorandum

4. TITLE AND SUBTITLE

Performance of the NASA 30 cm Ion Thruster

5. FUNDING NUMBERS

WU–506–42–31

6. AUTHOR(S)

Michael J. Patterson, Thomas W. Haag, and Scot H. Hovan

7. PERFORMING ORGANIZATION NAME(S) AND ADDRESS(ES)

National Aeronautics and Space Administration
Lewis Research Center
Cleveland, Ohio 44135–3191

8. PERFORMING ORGANIZATION REPORT NUMBER

E–8268

9. SPONSORING/MONITORING AGENCY NAME(S) AND ADDRESS(ES)

National Aeronautics and Space Administration
Washington, D.C. 20546–0001

10. SPONSORING/MONITORING AGENCY REPORT NUMBER

NASA TM–106426
IEPC–93–108

11. SUPPLEMENTARY NOTES

Prepared for the 23rd International Electric Propulsion Conference, cosponsored by the AIAA, AIDAA, DGLR, and JSASS, Seattle, Washington, September 13–16, 1993. Michael J. Patterson and Thomas W. Haag, NASA Lewis Research Center, and Scot A. Hovan, University of Dayton, Department of Mechanical Engineering, Dayton, Ohio 45469. Responsible person, Michael J. Patterson, (216) 433–7481.

12a. DISTRIBUTION/AVAILABILITY STATEMENT

Unclassified - Unlimited
Subject Category 20

12b. DISTRIBUTION CODE

13. ABSTRACT ***(Maximum 200 words)***

A 30 cm diameter xenon ion thruster is under development at NASA to provide an ion propulsion option for missions of national interest, and is being proposed for use on the USAF/TRW Space Surveillance, Tracking and Autonomous Repositioning (SSTAR) platform to validate ion propulsion. The thruster incorporates innovations in design, materials, and fabrication techniques compared to those employed in conventional ion thrusters. Specific development efforts include thruster design optimizations, component life testing and validation, vibration testing, and performance characterizations. Under this test program, the ion thruster will be brought to engineering model development status. This paper discusses the performance and power throttling test data for the NASA 30 cm diameter xenon ion thruster over an input power envelope of 0.7 to 4.9 kW, and corresponding thruster lifetime expectations.

14. SUBJECT TERMS

Ion thruster

15. NUMBER OF PAGES

27

16. PRICE CODE

A03

17. SECURITY CLASSIFICATION OF REPORT	18. SECURITY CLASSIFICATION OF THIS PAGE	19. SECURITY CLASSIFICATION OF ABSTRACT	20. LIMITATION OF ABSTRACT
Unclassified	Unclassified	Unclassified	

National Aeronautics and
Space Administration

Lewis Research Center
21000 Brookpark Rd.
Cleveland, OH 44135-3191